GRAIN SORTING, POROSITY, AND ELASTICITY

Jack Dvorkin and Mario A. Gutierrez
Geophysics Department, Stanford University

July 24, 2001

ABSTRACT

Grain size distribution (sorting) is determined by deposition. It may affect sediment bulk and elastic properties in a non-linear and non-unique way. The quantification of these relations is important for seismic reservoir characterization, especially in geological settings where sand/shale (bimodal) mixtures are present. Below, effective-medium equations are introduced for calculating the porosity and elastic moduli of such bimodal granular mixtures. These equations can be used for theoretical mixing of sand and shale in dispersed or laminar modes and, ultimately, for seismic forward modeling and reservoir characterization.

INTRODUCTION AND PROBLEM FORMULATION

Grain size and grain size distribution are basic characteristics of sediment texture (Figure 1). They are determined by the depositional history and affect reservoir quality via two of the most important bulk properties–porosity and permeability. They also affect the elastic properties of the sediment. As a result, seismic attributes can be, in principle, interpreted in terms of texture and porosity.

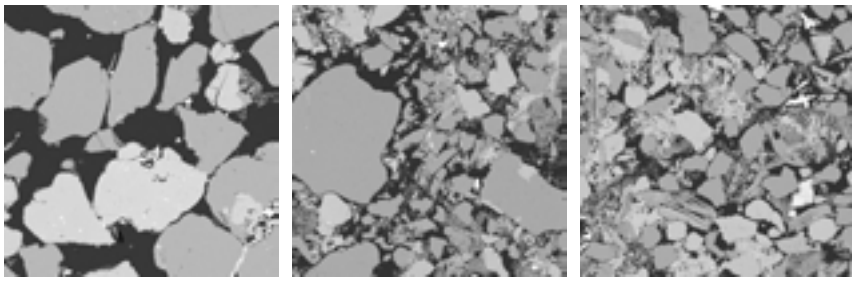

Figure 1. Thin sections of unconsolidated sand showing deteriorating sorting (from left to right). Images courtesy Norsk Hydro.

The effect of texture on sediment bulk and elastic properties is not simple. Consider a water-saturated section of a Gulf Coast well at a depth of about 900 m (Figure 2). The

section includes several depositional cycles whose vertical extent is apparent in the gamma-ray (GR) curve. The porosity curve approximately mirrors the GR curve, with high porosity matching the sandy (low-GR) zones. The *P*-wave impedance curve approximately mirrors the porosity curve with the low impedance matching high porosity.

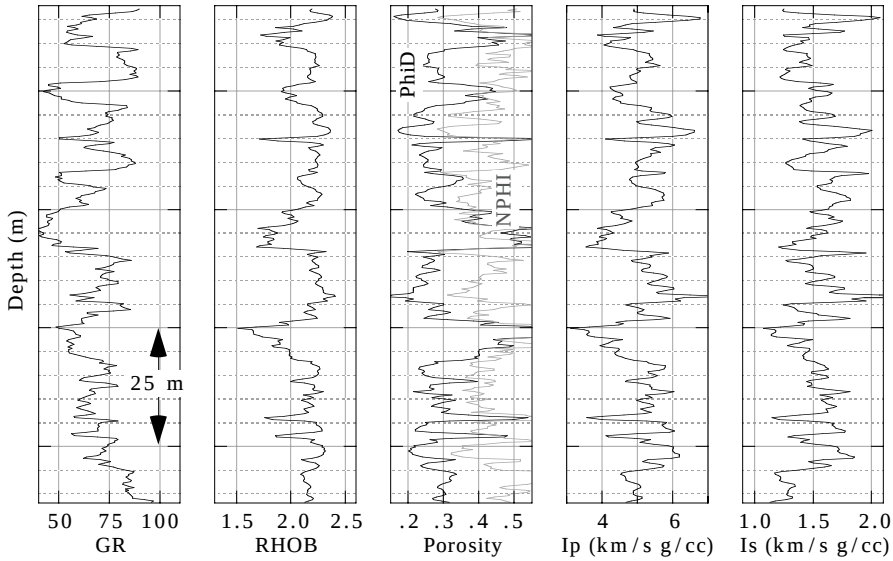

Figure 2. Well log curves for a Gulf of Mexico well. From left to right—GR; bulk density; density-derived porosity (PhiD) and neutron porosity (NPHI); *P*-wave impedance (Ip) and *S*-wave impedance (Is). Data courtesy Lake Ronel Oil Company.

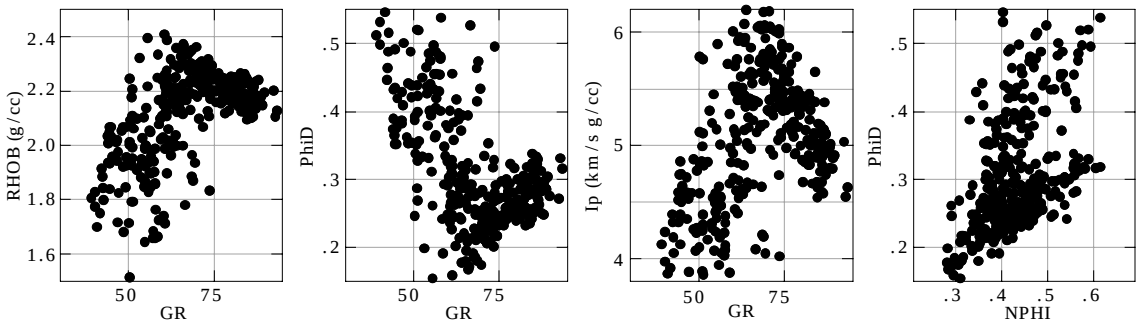

Figure 3. Cross-plots of well log data from Figure 2. Left to right: bulk density versus GR; density-derived porosity (PhiD) versus GR; *P*-wave impedance versus GR; and PhiD versus NPHI.

In spite of the congruency between different log curves apparent in Figure 2, the cross-plots of sediment properties do not produce unique trends (Figure 3). The increasing GR acts first to increase and then reduce the bulk density; reduce and increase porosity; and increase and reduce the impedance.

The elastic modulus versus porosity cross-plot also has two branches, in accord with

the changing GR values (Figure 4). Within the same porosity range, the shale-branch sediment is softer than the sand-branch sediment.

The *V*-shaped cross-plots, such as in Figure 3, second frame, are well-known in powder technology (Cumberland and Crawford, 1987). They result from mixing particles of two distinctively different mean sizes such that the small particles fill the pore space between the large particles (dispersed mixing). In the above field example these are the shale and sand particles, respectively.

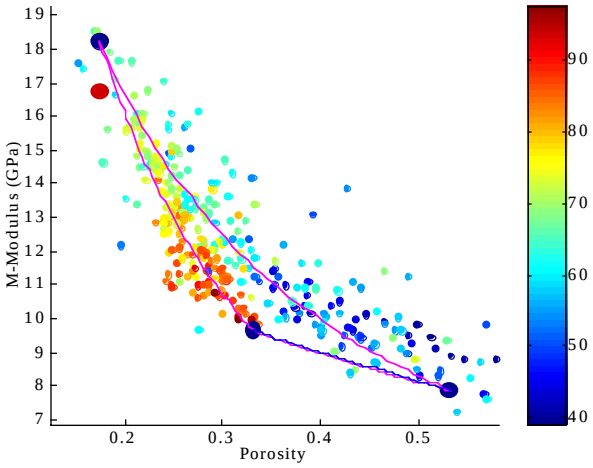

Figure 4. Compressional modulus (M-modulus), the product of bulk density and *P*-wave velocity squared, versus total porosity for data shown in Figure 2, color-coded by GR. The curves are from the sand/shale mixing theory. The large dark-blue symbols represent the pure sand and pure shale end points and for the critical concentration point (upper left corner). The large red symbol at the critical concentration point is from approximate Equation (19). The two laminar mixture curves that connect the pure sand and pure shale end points are from Equations (22) and (23) and are practically identical to each other.

This bimodal mixture effect clearly manifests itself in a synthetic data set of Estes (1992) where the porosity and elastic-wave velocities have been measured in mixtures of round glass beads of two sizes—0.5 and 0.05 mm (Figure 5). Porosity is approximately the same, and the elastic-wave velocities are approximately the same at the end points where the pack is made of either large or small grains. As the fraction of small grains increases, porosity first decreases from 0.38 to its minimum of 0.26 and then increases again to 0.36. Both *P*- and *S*-wave velocity first increase and then decrease. The maxima of the elastic-wave velocity corresponds to the porosity minimum.

The *V*-shaped cross-plots have been recognized in geophysics (Smith and Gidlow, 1987) and used, for example, for identifying clay-supported and framework-supported sediment domains (Herron et al., 1992). The *V*-shaped cross-plots of the density-derived porosity and neutron porosity (such as in Figure 2, right panel) appear as early as 1974 in the Schlumberger log interpretation manual.

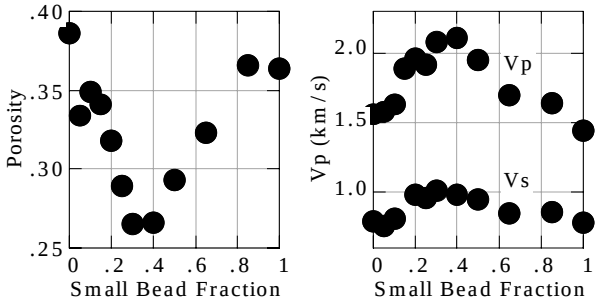

Figure 5. Mixtures of glass beads of two sizes, 0.5 and 0.05 mm. Porosity (left) and *P*- and *S*-wave velocity (right) versus the volume fraction of small beads. After Estes (1992).

Marion (1990) and Yin (1992) have developed the heuristic theory of *V*-shaped plots and supported it by laboratory measurements on synthetic geomaterials. The *V*-shaped plots resulting from Yin's (1992) measurements of the total porosity, elastic-wave velocity, and permeability in synthetic mixtures of Ottawa sand and kaolinite are shown in Figure 6.

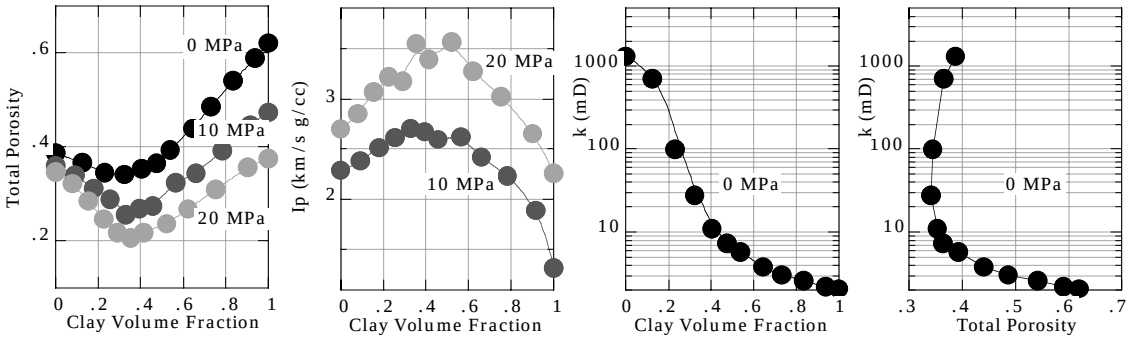

Figure 6. Mixtures of sand and clay. Measurements were conducted on room-dry samples at varying hydrostatic confining pressure (shown in the plots). From left to right—total porosity; *P*-wave impedance; air permeability versus volumetric clay content; and air permeability versus total porosity.

In this data set, both the *particle type* and its volumetric proportion in the mixture (which is relevant to geologic *sorting*), strongly affect the properties of the synthetic sediment in a non-linear and non-unique way. This effect will persist in situ where the

mineralogies of the sand and shale particles are, generally, different.

Being able to quantify the effect of sorting and sand/shale mixing on the bulk and elastic sediment properties is crucial for rational synthetic modeling of the seismic response of sand and shale sequences in situ. In turn, such synthetic models can be used to predict reservoir quality from real seismic attributes. One important target of such modeling are thin interbedded sand/shale layers in deep water sedimentary environments. A specific question is how to connect the porosity and velocity depth-trend curves for pure sand and pure shale, given the shale content.

To this end, the problem is posed to develop an effective-medium model for a mixture of particles of two distinctively different sizes (a bimodal mixture) that relates the total porosity to the content of the small particles in the mixture (shale content) and also relates the effective elastic moduli of the mixture to the content of the small particles; total porosity; effective pressure; and the pore-fluid bulk modulus.

TOPOLOGY OF BIMODAL MIXTURES—DISPERSED MODE

Consider two types of spherical grains of radii R and r, respectively, mixed in varying proportions. The two end members of such mixtures are the packs of only the large grains or only the small grains (Figure 7). The porosity of the former is ϕ_{SS} and that of the latter is ϕ_{SH}. The size of the large grains is much larger than that of the small grains ($R >> r$). As a result, the small grain packs can fit within the pore space of the large grain pack and still retain their local porosity of ϕ_{SH}. This mixing mode is the *dispersed* mode. It is the most compact way of mixing grains of different sizes.

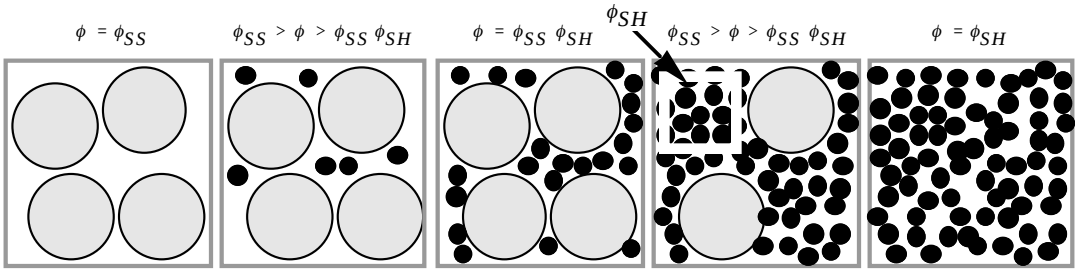

Figure 7. Dispersed mixing mode of large and small grains. The large-grain end member is on the far left and the small-grain end member is on the far right. The critical concentration point is in the middle. The total porosity is given above the frames. The fourth from the left frame shows a sub-volume of the small particles that retains the porosity of the small grain pack end member.

Depending on the proportion of the large and small grains, various mixture configurations are possible, as shown in Figure 7. The critical point in this figure is in the middle, where the small grains completely fill the pore space of the large grain pack and the large grains are still in contact with each other. Yin (1992) calls this configuration *critical concentration*. The importance of this middle point is that it separates two different structural domains. The domain on the left is where the external load applied to the mixture is born by the large grain framework. In the context of sand/shale mixtures, this is shaley sand. The domain on the right is where the large grains are suspended in the small particle framework which is now load-bearing. This is sandy shale.

Let the number of the large and small grains in the mixture be L and l, respectively. Then the total volume of the mixture V_t in the domain to the left of the critical concentration point (shaley sand) is that of the large grain pack (V_{tl}):

$$V_t = V_{tl} = (4/3)\pi R^3 L / (1 - \phi_{SS}), \tag{1}$$

The pore volume of the large grain pack is

$$V_{pl} = (4/3)\pi R^3 L \phi_{SS} / (1 - \phi_{SS}), \tag{2}$$

and the total volume of the small grains, counting the pore space between them, is

$$V_{ts} = (4/3)\pi r^3 l / (1 - \phi_{SH}). \tag{3}$$

In the context of sand/shale mixtures, the latter is the total shale volume in the sediment.

If $V_{ts} \le V_{pl}$, the small grains can fit into the pore space of the large grains without distorting the initial large grain framework. The pore volume of the mixture V_{pm} is the pore volume of the large grain pack V_{pl} minus the small grain material volume:

$$V_{pm} = V_{pl} - (4/3)\pi r^3 l. \tag{4}$$

As a result, the total porosity of the mixture ϕ is

$$\phi = \phi_{SS} - \beta(1 - \phi_{SH}), \quad \beta \le \phi_{SS}, \tag{5}$$

where

$$\beta = [r^3 l / (1 - \phi_{SH})] / [R^3 L / (1 - \phi_{SS})]. \tag{6}$$

For $\beta \le \phi_{SS}$, β is the volume fraction of shale C in the whole rock. In this $C \le \phi_{SS}$ domain, the total porosity decreases from its (pure sand) end-member value ϕ_{SS} to the

minimum (critical concentration) value of $\phi_{SS}\phi_{SH}$.

If $\beta > \phi_{SS}$, the large grains are suspended in the small grain pack. The total volume of the mixture now is the sum of the small grain pack volume and the large grain material volume:

$$V_t = (4/3)\pi R^3 L + (4/3)\pi r^3 l / (1 - \phi_{SH}). \quad (7)$$

The pore volume of the mixture is that of the small grain pack:

$$V_{pm} = (4/3)\phi_{SH}\pi r^3 l / (1 - \phi_{SH}). \quad (8)$$

As a result, the total porosity is

$$\phi = \phi_{SH} / [1 + (1 - \phi_{SS}) / \beta]. \quad (9)$$

The volume fraction of the small grain pack in the mixture is, in the sand/shale mixture context, the volume fraction of shale C in the whole rock. It is

$$C = [1 + (1 - \phi_{SS}) / \beta]^{-1}. \quad (10)$$

Then Equation (9) becomes $\phi = \phi_{cs}C$.

The summary of the above equations in the sand/shale mixture context is

$$\phi = \phi_{SS} - C(1 - \phi_{SH}), \quad C \le \phi_{SS}; \quad \phi = \phi_{SH}C, \quad C \le \phi_{SS}; \quad (11)$$

where ϕ_{SS} and ϕ_{SH} are the porosities of the pure sand and pure shale end-members, respectively.

The dry-rock bulk density ρ_{DRY} of the mixture is

$$\begin{aligned} \rho_{DRY} &= (1 - \phi_{SS})\rho_{SS} + C(1 - \phi_{SH})\rho_{SH}, \quad C \le \phi_{SS}; \\ \rho_{DRY} &= (1 - C)\rho_{SS} + C(1 - \phi_{SH})\rho_{SH}, \quad C > \phi_{SS}; \end{aligned} \quad (12)$$

where ρ_{SS} and ρ_{SH} are the sand and shale grain-material densities, respectively. To calculate the bulk density ρ_B of the sediment with pore fluid, the term $\phi\rho_F$, where ρ_F is the pore-fluid density, has to be added to ρ_{DRY}.

TOPOLOGY OF BIMODAL MIXTURES—LAMINAR MODE

The laminar mode of mixing is where the large grain packs and the small grain packs fill the space as separate entities without changing the topology of the pore space inside the packs (Figure 8). The geological realization of this mode is "laminar shale" where the shale is laminae between which are layers of sand (Schlumberger, 1989).

The total porosity of this mixture is simply the weighed average of the sand and shale porosities:

$$\phi = C\phi_{SH} + (1 - C)\phi_{SS}. \tag{13}$$

The bulk density is

$$\rho_B = (1 - C)[(1 - \phi_{SS})\rho_{SS} + \phi_{SS}\rho_{FSS}] + C[(1 - \phi_{SH})\rho_{SH} + \phi_{SH}\rho_{FSH}], \tag{14}$$

where ρ_{FSS} and ρ_{FSH} are the densities of the pore fluids in the sand and shale bodies, respectively.

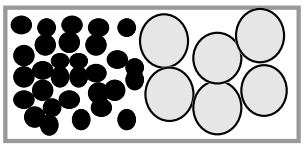

Figure 8. Laminar mode of large and small grains mixing.

The porosity dependence on the small grain (shale) content is non-linear and non-unique in the dispersed mode and linear in the laminar mode (Figure 9). The dispersed mode curve reproduces the *V*-shapes apparent in Figures 3, 5, and 6.

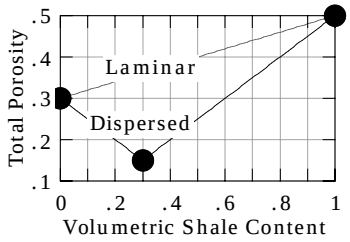

Figure 9. Total porosity versus shale content for dispersed and laminar modes of mixing. In this example, the pure-sand porosity is 0.3 and the pure-shale porosity is 0.5. The symbols indicate the end members (pure sand and pure shale) and the critical concentration point.

ELASTICITY OF BIMODAL MIXTURES—DISPERSED MODE

Assume that the effective bulk (K) and shear (G) moduli of the pure sand and pure shale end-members are known and are, respectively, K_{SS} and G_{SS} for sand, and K_{SH} and G_{SH} for shale. Also known are the grain material elastic moduli that are, respectively, K_1 and G_1 for the sand (large) grains, and K_2 and G_2 for the shale (small) grains.

Consider first *sandy shale* (the three right-hand frames in Figure 7) where the pack of the shale particles envelops the sand grains. The mixture under examination is a composite of two elastic elements—the softer element that is porous shale and the stiffer element that

is the sand grain material. The softer element envelops the stiffer element thus creating the topology that is a realization of the Hashin-Shtrikman lower bound (HSLB). Dvorkin et al. (1999) show that if the elastic contrast between the two elements is large, HSLB accurately predicts experimental measurements. The resulting expressions for the mixture's elastic moduli are:

$C \geq \phi_{SS}$:

$$K_{MIX} = \left[\frac{C}{K_{SH} + (4/3)G_{SH}} + \frac{1-C}{K_1 + (4/3)G_{SH}}\right]^{-1} - \frac{4}{3}G_{SH}, \qquad (15)$$

$$G_{MIX} = \left[\frac{C}{G_{SH} + Z_{SH}} + \frac{1-C}{G_1 + Z_{SH}}\right]^{-1} - Z_{SH}, \quad Z_{SH} = \frac{G_{SH}}{6}\frac{9K_{SH} + 8G_{SH}}{K_{SH} + 2G_{SH}},$$

where C is the volume shale content as given by Equation (10).

The Hashin-Shtrikman's are the tightest elastic bounds for an isotropic mixture of several elastic components. The Voigt-Reuss bounds are more relaxed. The lower (Reuss) bounds for the bulk and shear moduli are (Mavko et al., 1998):

$$C \geq \phi_{SS}: \quad K_{MIX} = [CK_{SH}^{-1} + (1-C)K_1^{-1}]^{-1}, \quad G_{MIX} = [CG_{SH}^{-1} + (1-C)G_1^{-1}]^{-1}. \qquad (16)$$

The *P*- and *S*-wave velocity (ultrasonic pulse transmission) measured by Yin (1992) in water-saturated pure kaolinite at 10 MPa hydrostatic effective pressure are V_P = 1.94 and V_S = 0.99 km/s, respectively. The corresponding bulk density is ρ_B = 1.83 g/cc. The resulting bulk and shear moduli are $K_{SH} = \rho_B[V_P^2 - (4/3)V_S^2]$ = 4.5 GPa and $G_{SH} = \rho_B V_S^2$ = 1.8 GPa, respectively. The bulk and shear moduli of pure quartz grains are K_1 = 36.6 GPa and G_1 = 45 GPa, respectively. Using these inputs, the sand/shale mixture elastic moduli are computed according to Equations (15) and (16) and plotted in Figure 10.

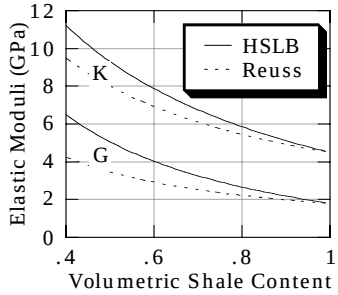

Figure 10. The effective bulk (*K*) and shear (*G*) moduli of the mixture of water-saturated kaolinite and quartz grains computed according to Equations (15) and (16). The results are for the sandy shale domain where the volumetric shale content exceeds the porosity of pure sand (about 0.4).

The difference between the HSLB and Reuss results is substantial, especially at the critical concentration point ($C = \phi_{SS} \approx 0.4$). HSLB equations are slightly more complicated than the Reuss equations, however they are more appropriate for an isotropic mixture of elastic elements and thus recommended for estimating the elastic moduli of sandy shale.

It is common in practical geophysics that the *S*-wave data are either not available or of questionable quality. In this case Equations (15) cannot be used because neither the bulk not the shear modulus can be calculated from V_P only. If the Poisson's ratio of the sand grain material and that of the pure shale are the same, $\nu_1 = \nu_{SH} \equiv \nu_*$, then by substituting isotropic elasticity equations

$$K = M\frac{1+\nu}{3(1-\nu)}, \quad G = M\frac{1-2\nu}{2(1-\nu)}, \quad M = K + \frac{4}{3}G \tag{17}$$

into Equations (15), HSLB for the compressional modulus of the mixture M_{MIX} can be expressed in terms of the compressional modulus of the sand grain material, $M_1 = K_1 + (4/3)G_1$, that of pure shale, $M_{SH} = K_{SH} + (4/3)G_{SH}$, and ν_*:

$$\begin{aligned}
&C \geq \phi_{SS}: \quad M_{MIX} = K_{MIX} + \frac{4}{3}G_{MIX};\\
&K_{MIX} = M_{SH}\{[C + \frac{3(1-C)(1-\nu_*)}{(1+\nu_*)(M_1/M_{SH}) + 2(1-2\nu_*)}]^{-1} - \frac{2(1-2\nu_*)}{3(1-\nu_*)}\},\\
&G_{MIX} = M_{SH}\frac{1-2\nu_*}{4(1-\nu_*)(4-5\nu_*)}\cdot\\
&\{[\frac{C}{15(1-\nu_*)} + \frac{1-C}{2(4-5\nu_*)(M_1/M_{SH}) + 7 - 5\nu_*}]^{-1} - (7-5\nu_*)\}.
\end{aligned} \tag{18}$$

It is not likely that $\nu_1 = \nu_{SH}$. Therefore, Equations (18) have to be treated as an approximation. M_{MIX} computed from these approximate equations is compared to that computed from the exact Equations (15) in Figure 11, left. It appears that although the Poisson's ratio of sand grains may be as low as 0.07 (pure quartz) and that of the water-saturated shale may be as high as 0.45, the error in using Equations (18) does not exceed 5% if the common Poisson's ratio ν_* is set close to ν_{SH}.

The correct choice for ν_* should be based on the knowledge of the elastic properties of shale in the region and depth range of interest. Very shallow shales typically have a very large Poisson's ratio that approaches 0.45. In deep shales, Poisson's ratio may be close to

0.3 (Figure 12). In uplifted sedimentary sequences, relatively low (~ 0.3) Poisson's ratio in shales may appear at shallow depths.

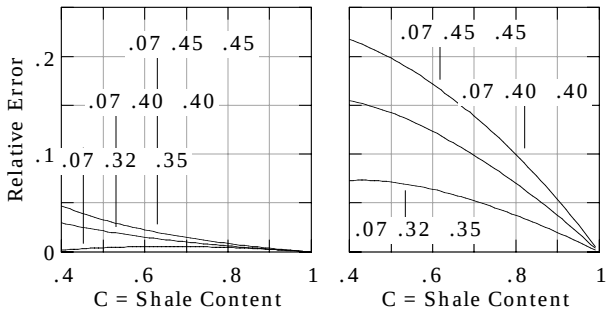

Figure 11. Left: The relative error of using Equations (18) instead of Equations (15) for the effective compressional modulus (M) of sandy shale. Right: The relative error of using Equation (19) instead of Equations (15) for the effective compressional modulus (M) of sandy shale. The triplets of numbers stand for ν_1, ν_{SH}, and ν_*. For example, the triplet (.07 .45 .45) means ν_1 = .07; ν_{SH} = .45; and ν_* = 0.45.

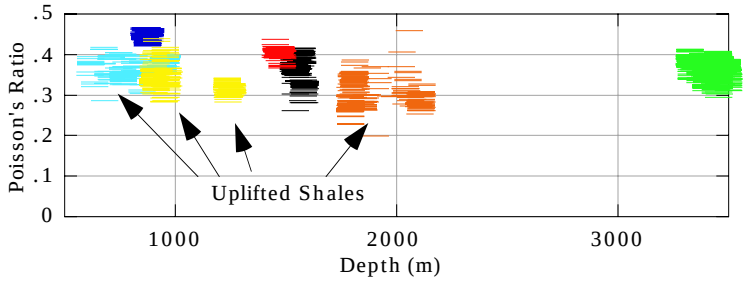

Figure 12. Poisson's ratio (as calculated from P- and S-wave log data) in shale versus depth for selected wells. Different color corresponds to different wells.

An alternative for V_P-only modeling is to use the Reuss weighted average (lower bound) for the compressional modulus:

$$C \geq \phi_{SS}: \quad M_{MIX} = [\frac{C}{M_{SH}} + \frac{1-C}{M_1}]^{-1}. \tag{19}$$

The relative error of using this equation instead of the exact Equations (15) may be unacceptably large (Figure 11, right).

Consider next *shaly sand* (the three left-hand frames in Figure 7) where the packs of the shale particles are located within the pore space of the undisturbed sand grain framework. Shaly sand can be treated as a mixture of two end members which are the pure sand and the critical concentration sand/shale mixture (Figure 13). Then the shaly sand

elastic moduli vary between those of the end members which are the moduli of pure sand (K_{SS} and G_{SS}) and of the critical concentration mixture (K_{CC} and G_{CC}) as given by Equations (15) at $C = \phi_{SS}$. The total porosity varies between ϕ_{SS} and $\phi_{SS}\phi_{SH}$, respectively. The volumetric concentration of the pure sand end member in shaly sand is $1 - C / \phi_{SS}$ while that of the critical concentration mixture is C / ϕ_{SS} (Figure 13).

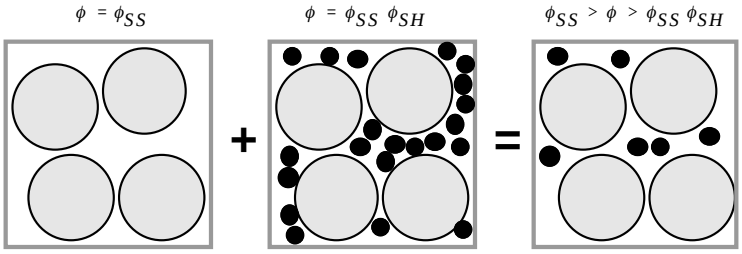

Figure 13. The sum of two end members (pure sand and critical concentration mixture) produces shaly sand.

In shaly sand, the shale particles fall in the pore space of the pure sand framework and do not significantly affect its stiffness. Therefore, in order to calculate the effective elastic moduli of shaly sand, it is logical to connect the elastic moduli of the end members by the HSLB curve where the soft end member is pure sand:

$C \le \phi_{SS}$:

$$K_{MIX} = \left[\frac{1 - C / \phi_{SS}}{K_{SS} + (4/3)G_{SS}} + \frac{C / \phi_{SS}}{K_{CC} + (4/3)G_{SH}}\right]^{-1} - \frac{4}{3}G_{SS}, \tag{20}$$

$$G_{MIX} = \left[\frac{1 - C / \phi_{SS}}{G_{SS} + Z_{SS}} + \frac{C / \phi_{SS}}{G_{CC} + Z_{SS}}\right]^{-1} - Z_{SS}, \quad Z_{SS} = \frac{G_{SS}}{6}\frac{9K_{SS} + 8G_{SS}}{K_{SS} + 2G_{SS}},$$

where K_{CC} and G_{CC} are K_{MIX} and G_{MIX}, respectively, as given by Equations (15) at $C = \phi_{SS}$. The Reuss weighted average for V_P-only modeling, similar to Equation (19) is

$$C \ge \phi_{SS}: \quad M_{MIX} = \left[\frac{1 - C / \phi_{SS}}{M_{SS}} + \frac{C / \phi_{SS}}{M_{CC}}\right]^{-1}, \tag{21}$$

where $M_{CC} = K_{CC} + (4/3)G_{CC}$.

The Reuss lower-bound may significantly differ from HSLB if the elastic contrast between the end members is large (e.g., the contrast between pure quartz and porous shale). However, if the elastic contrast is relatively small (as between pure sand and the critical concentration mixture), Equations (20) and (21) provide results that are close to each other. Therefore, the use of the Reuss bound is justified for the purpose of calculating the elastic

modulus of shaly sand.

ELASTICITY OF BIMODAL MIXTURES—LAMINAR MODE

In the laminar mode, the effective elastic moduli of the sand/shale mixture monotonically vary between those of the pure sand and pure shale end members. If the pure sand and pure shale bodies are arranged in an elastically isotropic configuration, the effective elastic moduli of the laminar mixture lie between the lower and upper Hashin-Shtrikman bounds (Mavko et al., 1998). In traditional geophysical applications, an elastic wave propagates approximately perpendicular to sand and shale layers. Such layered configuration is anisotropic. Its elastic constants are given by the Backus average (Mavko et al., 1998). The compressional elastic modulus in the direction perpendicular to the layers is simply the Reuss average of the moduli of the layers:

$$0 \le C \le 1: \quad M_{MIX} = [\frac{1-C}{M_{SS}} + \frac{C}{M_{SH}}]^{-1}. \tag{22}$$

The compressional modulus is the product of density and P-wave velocity. Therefore, Equation (22) is not equivalent to the popular Wyllie's travel time average:

$$0 \le C \le 1: \quad V_{P\_MIX} = [\frac{1-C}{V_{P\_SS}} + \frac{C}{V_{P\_SH}}]^{-1}, \tag{23}$$

where V_{P_MIX}, V_{P_SS}, and V_{P_SH} are for the *P*-wave velocity in the laminar sand/shale mixture, pure sand, and pure shale, respectively. However, if the elastic contrast between sand and shale is not large (which is very often the case), Equations (22) and (23) give essentially the same result (see Figure 15 below).

ELASTICITY OF PURE END MEMBERS

In many applications, the geophysicist will pick the elastic properties of pure sand and pure shale from well logs (see, e.g., curves in Figure 2 where the pure sand values and pure shale values correspond to the lowest and highest GR values in the interval, respectively). Afterwards, these end-member values can be used in the mixing equations given above.

In case where the elastic properties of the pure sand and shale end members are unknown, the uncemented (friable) sand equations (Dvorkin and Nur, 1996) based on the Hertz-Mindlin contact theory can be used to estimate those. The elastic moduli of the *dry*

frame of sand are

$$K_{SS\_Dry} = [\frac{n_{SS}^2(1-\phi_{SS})^2 G_1^{\,2}}{18\pi^2(1-\nu_1)^2} P]^{\frac{1}{3}}, \quad G_{SS\_Dry} = \frac{5-4\nu_1}{5(2-\nu_1)} [\frac{3n_{SS}^2(1-\phi_{SS})^2 G_1^{\,2}}{2\pi^2(1-\nu_1)^2} P]^{\frac{1}{3}}, \qquad (24)$$

where G_1 and ν_1 are the shear modulus and Poisson's ratio of the grain material, respectively; P is the effective pressure that is the difference between the overburden and pore pressure; and n_{SS} is the coordination number (the average number of contacts per grain). The coordination number depends on porosity. Its upper bound can be estimated from an empirical equation (after Murphy, 1982)

$$n_{SS} = 20 - 34\phi_{SS} + 14\phi_{SS}^2, \qquad (25)$$

where porosity is in fractions of unity. The spread of data below this curve may reach 2 (Figure 14). Eventually, the coordination number has to be calibrated by adjusting model results to site-specific data with Equation (25) serving as a guideline.

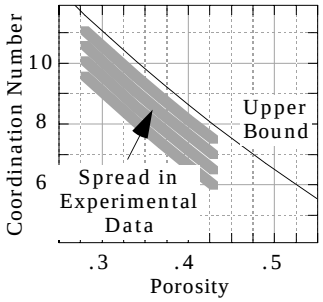

Figure 14. Coordination number versus porosity. The solid black curve is from Equation (25). The gray domain shows possible spread in coordination number values below the upper bound given by Equation (25).

The elastic moduli of *saturated* sand are calculated from those of the dry frame via Gassmann's (1951) equations:

$$K_{SS} = K_1 \frac{\phi_{SS} K_{SS\_Dry} - (1+\phi_{SS}) K_F K_{SS\_Dry} / K_1 + K_F}{(1-\phi_{SS}) K_F + \phi_{SS} K_1 - K_F K_{SS\_Dry} / K_1}, \quad G_{SS} = G_{SS\_Dry}, \qquad (26)$$

where K_1 and K_F are the bulk moduli of the grain material and pore fluid, respectively.

The elastic moduli of the grain material can be calculated from those of the mineral constituents via ad-hoc Hill's average:

$$M = \frac{1}{2}[\sum_{i=1}^{m} f_i M_i + (\sum_{i=1}^{m} f_i M_i^{-1})^{-1}], \tag{27}$$

where M is either bulk or shear modulus; subscript i stands for i-th mineral constituent; and m is the number of mineral constituents.

Shale is not a granular composite such as sand. Therefore, the validity of applying Equations (24) to pure shale is not obvious. However, there is evidence that these equations provide reasonable elastic property estimates (see Gutierrez et al., 2001, and example below). To use Equations (24) in the pure shale case, the subscript "SS" has to be replaced by "SH" and the shale grain elastic moduli G_2, ν_2, and K_2 have to be used instead of G_1, ν_1, and K_1.

APPLYING ROCK PHYSICS THEORY

Figure 4 shows the results of applying the sand/shale mixture equations to the log data from Figure 2. Both the pure sand and pure shale end members were picked from the compressional modulus versus porosity cross plot. The dispersed-shale theoretical curves were calculated from Equations (18) and (21). The value of M_1 was 100 GPa (pure quartz) and the value of ν_* was 0.45, according to the original log data.

Equation (19) was also used to calculate the compressional modulus at the critical concentration point. The result falls below the value given by Equation (18) but still gives a reasonable estimate for the elastic modulus at critical concentration and, in principle, can be used for modeling.

The laminar shale curve was calculated from the Backus average, as given by Equation (22), and also from Wyllie's time average, as given by Equation (23). The two results are practically identical.

The next example is from a vertical well in La Cira Field in Colombia (Gutierrez, 2001). These well log data span a depth interval from 150 to 600 m that includes shale sequences and fluvial sand bodies. The compressional modulus that is plotted versus total porosity in Figure 15 exhibits the familiar dispersed-shale *V*-shape.

In this example, Equations (24) – (26) were applied directly, without picking the end-member elastic properties from the cross-plot. It was assumed that the sand grains were quartz, with K_1 = 37 GPa and G_1 = 45 GPa, and the shale grains were clay with K_2 = 21 GPa and G_2 = 8 GPa (see Mavko et al., 1998, for mineral elastic moduli). The pure sand

and pure shale end-member porosity values have been selected as ϕ_{SS} = 0.3 and ϕ_{SH} = 0.2, respectively. The corresponding coordination number values from Equation (25) are n_{SS} = 11 and n_{SH} = 14, respectively. The bulk modulus of the water in the pore space was 2.5 GPa, calculated according to the site-specific salinity.

The results of modeling using the effective pressure of 2 MPa (for the shallow part of the interval under examination) and 10 MPa (for the deep part) are superimposed on the data in Figure 15. The dispersed shale *V*-shaped curves accurately mimic the data.

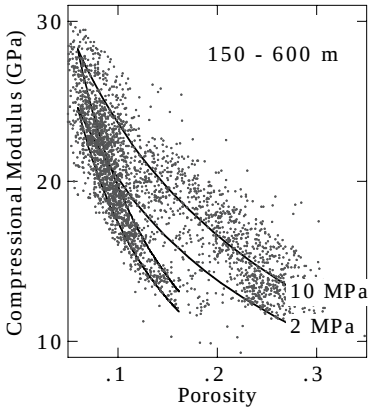

Figure 15. Compressional modulus versus total porosity for a La Cira well. The depth interval spans from 150 to 600 m. The two dispersed shale *V*-shaped theoretical curves are shown for the effective pressure of 2 and 10 MPa.

DEPTH TRENDS

Compaction in sedimentary basins acts to reduce the total porosity of sand and shales. Traditionally, the effect of compaction on porosity ϕ has been approximated by an exponent

$$\phi = \phi_0 e^{-aZ}, \tag{28}$$

where Z is depth; ϕ_0 is porosity at Z = 0; and a is a fitting coefficient. The coefficients in Equation (28) are site-specific. Also, in uplifted and eroded environments, Z = 0 may not correspond to the current-time zero depth and may be, in fact, negative.

According to Allen and Allen (1990), compaction coefficients appropriate for North Sea basins are ϕ_0 = 0.63 and a = 0.51 km^{-1} for shale, and ϕ_0 = 0.49 and a = 0.27 km^{-1} for sand. These parameters were used to construct the porosity versus shale content and depth trend shown in Figure 16, left, for both dispersed and laminar mixing modes.

The corresponding velocity trends for shale and sand end members can be determined from site-specific well log data or theoretically estimated from Equations (24). The result of the latter approach is shown in Figure 16, right.

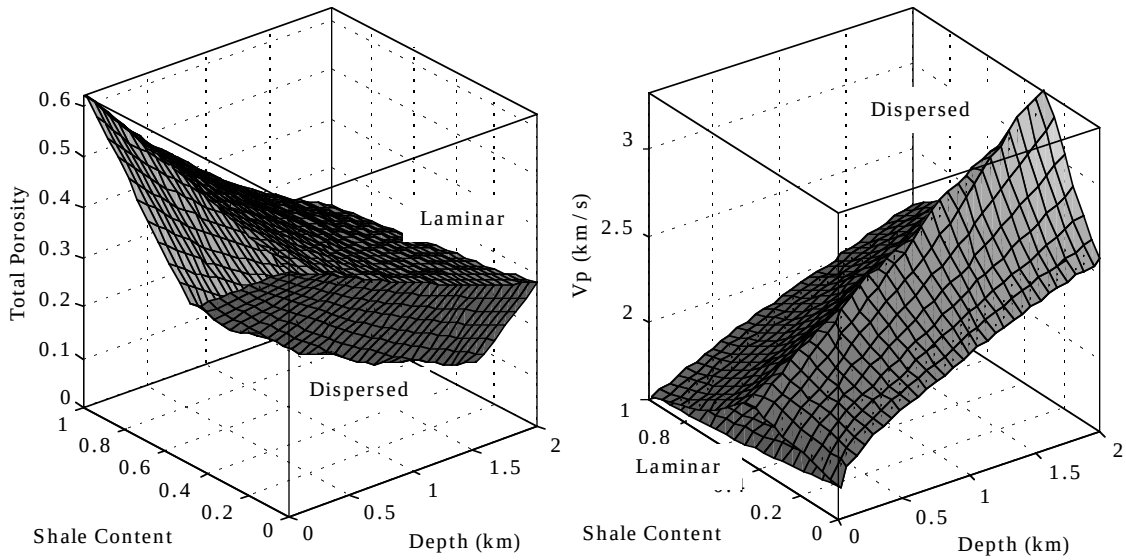

Figure 16. Total porosity (left) and *P*-wave velocity (right) versus depth and shale content. Inputs for the elastic property modeling are the same as in the example shown in Figure 16. The two-branch surfaces are for the dispersed shale mode. The intersections of these surfaces with the vertical planes of zero and 100% shale content give the pure sand and pure shale compaction curves, respectively. These curves are connected by single-branch laminar mode surfaces.

CONCLUSION

Sand and shale sequences, often charged with hydrocarbons, become visible to the geophysicist if illuminated by seismic radiation. The resulting seismic images are useful as long as they can be transformed into the images of porosity, lithology, pore fluid, and pore pressure. A way of obtaining such transforms is by relating the reservoir bulk properties and conditions to the elastic properties, forward modeling the response to seismic radiation, and comparing the synthetic seismograms to real reflection data.

Data show that the elastic and bulk properties of sand/shale mixtures depend on the mixing mode which may make the mixture very unsimilar to the initial end members, in all respects. The above examples of the effect of this complexity on density, porosity, and elastic-wave velocity are supplemented by sand/shale permeability data (Figure 6).

Fortunately, the complex and often confusing projections of natural events into the human mind often result from simple and logical laws. Once these laws are understood, they can be rationalized in mathematically simple ways and offered for practical usage. The equations presented in this paper give an example of such rationalization. They can be used for designing rock physics transforms between the elastic and bulk properties of sand/shale depositional sequences and, eventually, creating porosity and lithology volumes from volumes of seismic data.

ACKNOWLEDGMENT

This work was supported by Phillips Petroleum and the Stanford Rock Physics Laboratory. The data was provided by Lake Ronel Oil Company, Ecopetrol, and Norsk Hydro.

REFERENCES

Allen, P., and Allen, J., 1990, Basin analysis: Principles and applications, Blackwell.

Cumberland, D.J., and Crawford, R.J., 1987, The packing of particles, Handbook of powder technology, Elsevier.

Dvorkin, J., and Nur, A., 1996, Elasticity of High-Porosity Sandstones: Theory for Two North Sea Datasets, Geophysics, 61, 1363-1370.

Dvorkin, J., Berryman, J., and Nur, A., 1999, Elastic moduli of cemented sphere packs, Mechanics of Materials, 31, 461-469.

Estes, C.A., 1992, Personal communication.

Gassmann, F., 1951, Elasticity of porous media--Uber die elastizitat poroser medien, Vierteljahrsschrift der Naturforschenden Gesselschaft, 96, 1-23.

Gutierrez, M.A., Dvorkin, J., and Nur, A., 2001, Textural sorting effect on elastic velocities, Part I: Laboratory observations, rock physics models, and application to field data, SEG 2001, Expanded Abstracts.

Gutierrez, M.A., 2001, Rock physics and 3D seismic characterization of reservoir heterogeneities to improve recovery efficiency, Ph.D. thesis, Stanford University.

Herron, S.L., Herron, M.M., and Plumb, R.A., 1992, identification of clay-supported and framework-supported domains from geochemical and geophysical well log data, SPE 24726, 667-680.

Marion, D., 1990, Acoustical, mechanical, and transport properties of sediments and granular materials, Ph.D. thesis, Stanford University.

Mavko G., T. Mukerji and J. Dvorkin, 1998, The rock physics handbook, Tools for seismic analysis in porous media, Cambridge University Press.

Murphy, W.F., 1982, Effects of microstructure and pore fluids on the acoustic properties of granular sedimentary materials, Ph.D. thesis, Stanford University.

Smith, G.C., and Gidlow, P.M., 1987, Weighted stacking for rock property estimation and detection of gas, Geophysical Prospecting, 35, 993-1014.

Schlumberger, 1974, Log Interpretation, Volume II—Applications, Schlumberger Limited.

Schlumberger, 1989, Log Interpretation Principles/Applications, Schlumberger Wireline and Testing.

Yin, H., 1993, Acoustic velocity and attenuation of rocks: Isotropy, intrinsic anisotropy, and stress induced anisotropy, Ph.D. thesis, Stanford University.